Penning ionization electron spectroscopy of C6H6 by collision with He*(23S) metastable atoms and classical trajectory calculations: Optimization of ab initio model potentials

doi: 10.1063/1.1834900

Penning ionization electron spectroscopy of C_6H_6 by collision with He*($2\,^3S$) metastable atoms and classical trajectory calculations: Optimization of *ab initio* model potentials

Masakazu Yamazaki, Satoshi Maeda, Naoki Kishimoto, and Koichi Ohno[a)]
Department of Chemistry, Graduate School of Science, Tohoku University, Aramaki, Aoba-ku, Sendai 980-8578, Japan

(Received 13 August 2004; accepted 27 October 2004; published online 4 January 2005)

The potential energy surface of benzene (C_6H_6) with a He*($2\,^3S$) atom was obtained by comparison of experimental data in collision-energy-resolved two-dimensional Penning ionization electron spectroscopy with classical trajectory calculations. The *ab initio* model interaction potentials for C_6H_6+He*($2\,^3S$) were successfully optimized by the overlap expansion method; the model potentials were effectively modified by correction terms proportional to the overlap integrals between orbitals of the interacting system, C_6H_6 and He*($2\,^3S$). Classical trajectory calculations with optimized potentials gave excellent agreement with the observed collision-energy dependence of partial ionization cross sections. Important contributions to corrections were found to be due to interactions between unoccupied molecular orbitals and the He*2*s* orbital. A C_6H_6 molecule attracts a He*($2\,^3S$) atom widely at the region where π electrons distribute, and the interaction of -80 meV (ca. -1.8 kcal/mol) just cover the carbon hexagon. The binding energy of a C_6H_6 molecule and a He* atom was 107 meV at a distance of 2.40 Å on the sixfold axis from the center of a C_6H_6 molecule, which is similar to that of C_6H_6+Li and is much larger than those of the C_6H_6+[He,Ne,Ar] systems. © *2005 American Institute of Physics.* [DOI: 10.1063/1.1834900]

I. INTRODUCTION

Interactions of a molecule with an atom are of great importance in connection with many aspects in chemical physics, cluster science, organometalic chemistry, and biological science. Although interaction potentials for very simple systems such as linear molecules with an atom have been studied extensively, determinations of interaction potentials for larger systems have been rather scarce because of both experimental and theoretical difficulties. However, an interacting system involving aromatic π rings has attracted much interest. The geometries and stabilization energies for benzene and alkali atoms have been studied by matrix isolated IR spectroscopy[1] as well as by some theoretical calculations.[2,3] Recently, molecular beam scattering experiments of total cross sections have been successfully made for collisions of a benzene molecule with a rare gas (Rg) atom;[4] semiempirical interaction formulas[5] have been successful to account for the experimental findings. A harmonic expansion of the interaction potentials leading to the separation of the radial and angular dependencies was used to express the potential energy surfaces for C_6H_6+(He,Ne,Ar,Kr, or Xe).[6]

Another type of experiment that may lead to determination of anisotropic interaction potentials is collision-energy/electron-energy-resolved two-dimensional Penning ionization electron spectroscopy (2D-PIES),[7] which provides collision-energy dependence of partial ionization cross sections (CEDPICS) (Refs. 8 and 9) and collision-energy-resolved Penning ionization electron spectra (CERPIES).[10–12] Penning ionization occurs as collisional ionization of a molecule M in interaction with a metastable rare gas atom Rg* (Rg*+$M\rightarrow$Rg+M_i^++e^-). When a He*($2\,^3S$) atom (the excitation energy $E^*=19.82$ eV) is used as Rg*, ionization into a final ionic state M_i^+ takes place with a high probability when the 1*s* orbital of the He atom overlaps effectively with the target molecular orbital (MO) ϕ_i from which an electron is removed.[13] Since Rg* cannot penetrate into the repulsive wall, partial ionization cross sections become approximately proportional to exterior electron densities of respective MOs to be ionized.[14,15] Thus the most reactive geometries for Penning ionization are governed by the electron distributions of the target MO. Due to this characteristic reactivity, the interaction potentials around the spatially limited region can be reflected in collision-energy dependence, even in random collision experiments. Negative collision-energy dependence in CEDPICS is related to attractive interactions causing deflection of collision trajectories into potential well regions, which increases ionization probabilities especially in the lower collision energy E_c.[16] When attractive interactions are not important, repulsive boundaries limit the spatially accessible regions of Rg* to result in a positive E_c dependence in CEDPICS, because the larger E_c causes turning points of collision trajectories into the inner regions where target electron densities are highly distributed. Thus, CEDPICS for several ionic states gives information on the anisotropic interactions between a molecule and a He*($2\,^3S$) atom. Attractive interactions of He*($2\,^3S$) with π electron systems such as benzene[11,17,18] and substituted benzenes[19–23] have been disclosed by 2D-PIES technique. However, theoretical calculations on the col-

a)Author to whom correspondence should be addressed. Electronic mail: ohnok@qpcrkk.chem.tohoku.ac.jp

lision dynamics have not been made for these systems, and detailed anisotropic characteristics of the interaction potential surfaces are remained to be unknown.

Two important factors in the theory of Penning ionization are the ionization width Γ and the entrance potential of the reaction V^*.[24] Theoretical calculations have been made for relatively simple molecules such as H_2,[25] N_2,[12,26] and H_2O.[27] A semiempirical potential surface has been used for $Ne^* + CH_3Cl$.[28] Since the electronic state with a large excitation energy of a He atom is embedded in continuum states higher than the ionization threshold of the target molecule, *ab initio* calculations of Γ and V^* are in general very difficult. However, the difficulty for estimating V^* can be removed by using the well known similarity of a rare gas atom Rg* to a respective alkali metal atom with the same valence electron.[29,30] CEDPICS for $He^*(2\,^3S) + N_2$ has been successfully calculated by classical trajectory calculations based on $Li + N_2$ model potential and ionization widths for various ionic states estimated from overlap integrals.[31] Similar calculations were also performed for $He^*(2\,^3S) + CH_3CN$.[32] Replacement of Rg* by a respective alkali atom has also been made for interaction potentials of $Ar^* + CHCl_3$.[33]

In order to obtain interaction potentials by experiment, the interaction potential surface should be optimized to reproduce experimental features. Li model potentials for $He^*(2\,^3S) + (N_2, CO)$ have been improved by using an exponential function combined with Legendre polynomials.[34,35] However, the Legendre expansion suffers a very slow convergence in optimization, when the system becomes much larger and more highly anisotropic. Since intermolecular interactions are more or less related to overlaps of wave functions between the interacting species, corrections of model potentials can be expanded in terms of overlap integrals between MOs. In $He^*(2\,^3S) + (N_2, CO, C_2H_2, OCS)$, the radial and angular dependences of the overlap integrals between an *s*-type function and the target MOs were found to be successful for improving the Li-model potentials.[36,37] Since the overlap expansion method inherently takes anisotropies of the interacting system into account, it is a promising method to describe highly anisotropic interactions of large molecular systems.

In this paper, the improvement of *ab initio* Li model potentials by using the overlap expansion (OE) method[36] was first demonstrated for the nonlinear target molecule C_6H_6. Benzene is chosen, partly because it involves anisotropic repulsion and attraction around the molecule,[11,17,18] and also because a dimer of $C_6H_6 + Li$ (Refs. 1–3) is an interesting system, based on the similarity between $Li(2\,^2S)$ and $He^*(2\,^3S)$ atoms.

II. EXPERIMENTAL SECTION

The experimental apparatus used in the present study has been reported in previous papers.[8,9] A metastable beam of He was produced by a nozzle discharge source, and the $He^*(2\,^1S)$ component was quenched by a water-cooled helium discharge lamp. The metastable $He^*(2\,^3S)$ beam was pulsed by a mechanical chopper and then introduced into a collision cell located 504 mm downstream from the chopper disk. The kinetic energy of electrons ejected during the Penning ionization was measured by a hemispherical electrostatic deflection type analyzer using an electron collection angle 90° to the incident $He^*(2\,^3S)$ beam. The transmission efficiency curve of the electron-energy analyzer was determined by comparing our He I ultraviolet photoelectron spectra (UPS) data with those of Gardner and Samson[38] and Kimura *et al.*[39] The energy resolution of the electron-energy analyzer was 200 meV estimated from the full width at half maximum (FWHM) of the $Ar^+(^2P_{3/2})$ peak in the He I UPS. The background pressure in the reaction chamber was on the order of 10^{-7} Torr, and the experiments were performed under a sample pressure of ca. 2×10^{-5} Torr.

The He* velocity distribution $I_{He*}(v_{He*})$ was obtained by measuring the time-of-flight (TOF) of He* from the mechanical chopper to the collision cell which can be obtained by the detection of electrons emitted from a stainless steel plate inserted into the collision cell, since TOF of secondary electrons from the metal surface to the detector are negligibly short in comparison with that of the He* atoms. The 2D Penning ionization electron intensity of sample molecules $I_e(E_e, t)$ as functions of electron kinetic energy E_e and time t was converted to $I_e(E_e, \tau_{TOF})$ as functions of E_e and TOF of the He* beam. The $I_e(E_e, \tau_{TOF})$ can be lead to $I_e(E_e, v_{He*})$ as functions of E_e and velocity of He* atoms v_{He*}. By the following equations, the 2D Penning ionization cross section $\sigma(E_e, v_r)$ was obtained,

$$\sigma(E_e, v_r) = c\frac{I_e(E_e, v_{He*})}{I_{He*}(v_{He*})}\frac{v_{He*}}{v_r}, \tag{1}$$

$$v_r = \sqrt{v_{He*}^2 + \frac{3k_BT}{m}}, \tag{2}$$

where c is a constant, v_r is the relative velocity averaged over the velocity of the target molecule, k_B is the Boltzmann constant, and T and m are the gas temperature and the mass of the target molecule, respectively. The cross section in Eq. (1) is normalized by using the velocity distribution of He* beam $I_{He*}(v_{He*})$. Finally, $\sigma(E_e, v_r)$ is converted to $\sigma(E_e, E_c)$ by the relation

$$E_c = \tfrac{1}{2}\mu v_r^2, \tag{3}$$

where μ is the reduced mass of the colliding system. CEDPICS can be obtained by integrating 2D-PIES cross sections $\sigma(E_e, E_c)$ over the E_e range related to each ionic state.

In order to estimate branching ratios between produced ionic states, PIES at seven collision energies were deconvoluted with the following asymmetric Gaussian functions corresponding to each ionic band:

$$I_e(x, E_c) = \begin{cases} A(E_c)\exp[-\beta_1(x-E_0)^2] & \text{for } x < E_0 \\ A(E_c)\exp[-\beta_2(x-E_0)^2] & \text{for } x > E_0 \end{cases}, \tag{4}$$

where $A(E_c)$, E_0, β_1, and β_2 are parameters to be determined for each ionic band. Figure 1 displays the fitted results. Solid lines obtained by summations of asymmetric Gaussian functions almost agreed with experimental data plotted with circles. First, asymmetric widths (β_1 and β_2) and peak position E_0 of each Gaussian function were determined by a least-squares method for PIES at $E_c = 193$ meV. For the PIESs at the other energies, the widths

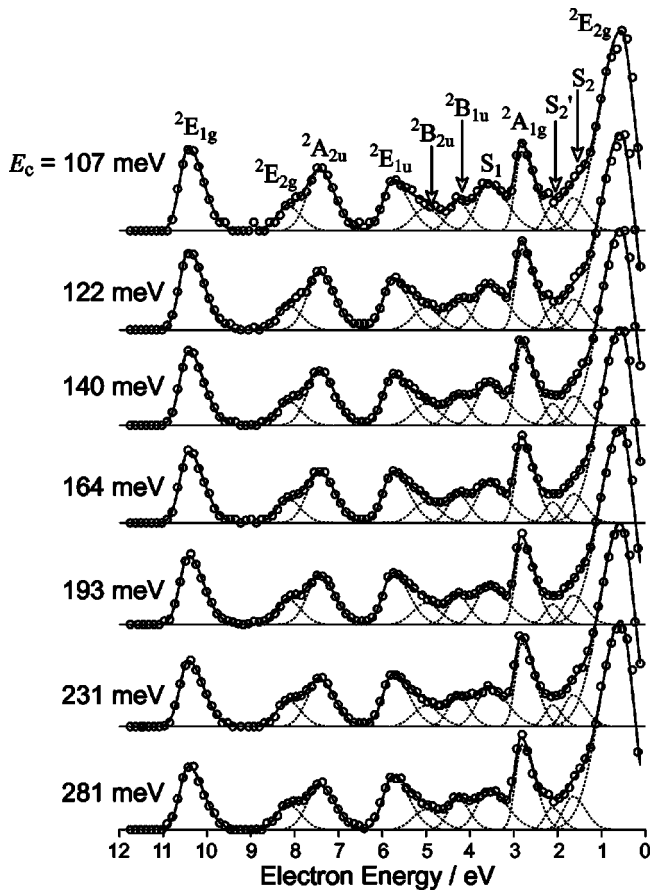

FIG. 1. Deconvolution of Penning ionization electron spectra at some collision energies. Experimental data are plotted with circles and deconvoluted band shapes are drawn with dashed lines. Summations of asymmetric Gaussian functions are shown with solid lines.

and peak positions were fixed at those obtained from PIES at $E_c = 193$ meV and the intensities $A(E_c)$ of each band were fitted. Although band shape and position in PIES may varies with E_c, its changes were found to be negligibly small for the system in this study as shown in Fig. 1.

III. METHOD OF CALCULATIONS

A. Entrance potential energy surface

It is difficult to obtain reliable interaction energies by the *ab initio* treatments of He*$(2\,^3S)$ associated with highly excited electronic states embedded in ionization continua. Based on the similarity between He*$(2\,^3S)$ and Li$(2\,^2S)$,[29,30] a ground state Li atom instead of a He*$(2\,^3S)$ atom can be used in calculations of the approximate potentials V_{Li} for V^*. In the present study, the Li-model potential V_{Li} should be improved by a reasonable manner to give better agreement with experiments. *Ab initio* MO calculations were performed on a GAUSSIAN program[40] by the second-order Møller-Plesset perturbation theory (MP2) with 6-311++G** basis set for C_6H_6+Li. Interaction model potential energy V_{Li} can be obtained in the following manner:

$$V_{\mathrm{Li}} = E_{\mathrm{MLi}} - (E_{\mathrm{M}} + E_{\mathrm{Li}}). \tag{5}$$

Here, E_{MLi}, E_{M}, and E_{Li} are the total energy of the supermolecule (MLi), the isolated molecule (M), and the isolated Li atom, respectively. The full counterpoise method[41] was employed to correct the basis set superposition error. The molecular structure was fixed at the experimental equilibrium geometry, and then the interaction potential $V_{\mathrm{Li}}(R,\theta,\phi)$ becomes a function of R, θ, and ϕ, where R is the distance between a Li(He*) atom and the center of mass of the target molecule, θ denotes the polar angle from the principal axis (C_6 axis for C_6H_6), and ϕ represents the azimuthal angle. *Ab initio* interaction energies of C_6H_6+Li were calculated at 267 independent sampling points, $\approx$15 points of different R and every 15° of θ and ϕ.

Although Li$(2\,^2S)$ has the same outer valence electronic configuration as He*$(2\,^3S)$ with a $2s$ electron that mainly contributes to the interactions, orbital interactions between Li$(2\,^2S)$ with a target molecule may be quantitatively different from those of He*$(2\,^3S)$. Therefore, it is efficient to modify V_{Li} according to the overlap between molecular orbitals. This OE method has recently proposed.[36] In the OE method, calculated model potentials V_{Li} can be modified with the following equations to obtain the V^* for He*$(2\,^3S)$:

$$V^*(R,\theta,\phi) = V_{\mathrm{Li}}(R,\theta,\phi) - \sum_i C_i |\langle \phi_i | \chi_s \rangle|^2, \tag{6}$$

$$\chi_s(r) = (\zeta^3/\pi)^{1/2} \exp(-\zeta r). \tag{7}$$

Here, ϕ_i is the ith target MO and χ_s is a normalized Slater-type orbital with exponent ζ which centered on a He*$(2\,^3S)$ atom. In the present study, ζ was set to be the He $2s$ orbital exponent of 0.575 bohr^{-1} determined by Slater's rule. The coefficients C_i are the potential parameters to be optimized. Figure 2 lists the numbering of ϕ_i and C_i for considered MOs of C_6H_6; lowest π and σ type unoccupied ($1e_{2u}$,$4a_{1g}$,$4e_{1u}$) and higher occupied ($1e_{1g}$, $3e_{2g}$, $1a_{2u}$, $3e_{1u}$, and $1b_{2u}$) MOs. The cutting planes for the electron density contour curves of the MOs are 1.0 Å away from the σ_h plane of a benzene molecule. MOs were obtained from *ab initio* self-consistent field (SCF) calculations with 6-311++G** basis set.

B. Ionization widths

The ionization width $\Gamma^{(i)}$ for producing the ith ionic state is given by

$$\Gamma^{(i)} = 2\pi\rho^{(i)} |\langle \Phi_0 | H_{\mathrm{el}} | \Phi^{(i)} \rangle|^2, \tag{8}$$

where $\rho^{(i)}$ is the density of the final state, H_{el} is the electronic Hamiltonian, and Φ_0 and $\Phi^{(i)}$ are the electronic wave function for the initial and final states, respectively. By using Slater determinant wave functions composed of the same one-electron orbitals for both initial and final states, we obtain for He*$(2\,^3S)$,

$$\langle \Phi_0 | H_{\mathrm{el}} | \Phi^{(i)} \rangle \approx \langle \chi_{2s}(1)\phi_i(2) | \frac{1}{r_{12}} | \chi_{1s}(2)\chi_{\varepsilon^{(i)}}(1) \rangle, \tag{9}$$

where χ_{2s} and ϕ_i are the $2s$ orbital of He* and the ith orbital of the target molecule, respectively, and χ_{1s} and $\chi_{\varepsilon^{(i)}}$ are the He $1s$ orbital and the ejected electron orbital, respectively. Miller and Morgner factored $\langle \chi_{2s}(1) | \chi_{\varepsilon^{(i)}}(1) \rangle$ out of the two-electron integral and simplified the two-electron integral

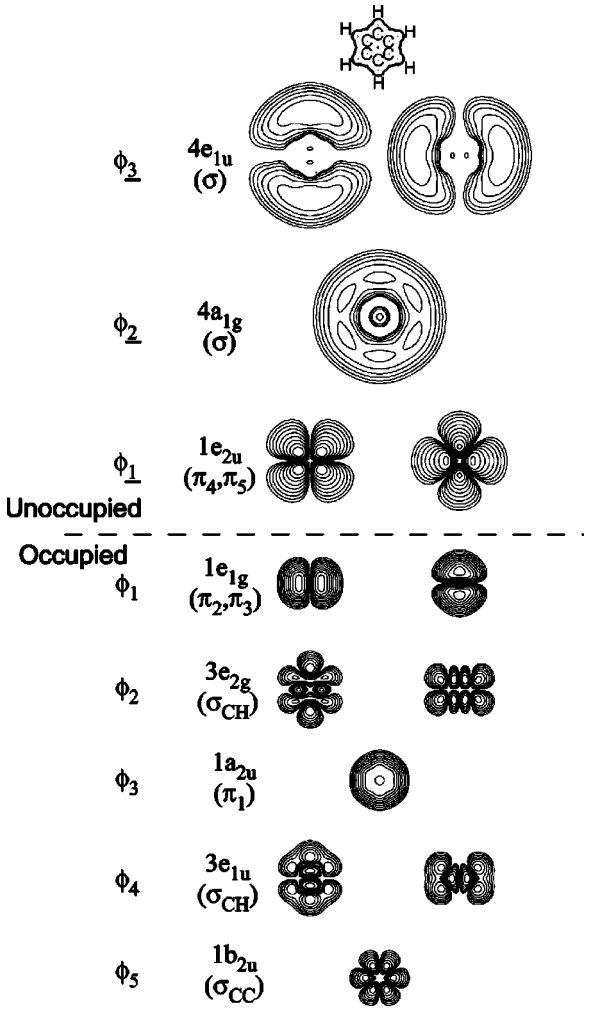

FIG. 2. Electron density contours of MOs of C_6H_6. Unoccupied MOs ($4e_{1u}$, $4a_{1g}$, $1e_{2u}$) and occupied MOs ($1e_{1g}$, $3e_{2g}$, $1a_{2u}$, $3e_{1u}$, and $1b_{2u}$) were used for potential optimization procedure (see Sec. III A).

by physical intuition rather than by a rigorous derivation.[42] The two-electron integral in Eq. (9) can be approximated as a product of two overlap integrals by employing widely used treatment in semiempirical molecular orbital theories[43] as well as in electron transport phenomena,[44]

$$-C\langle\phi_i|\chi_{1s}\rangle\langle\chi_{?s}|\chi_{\varepsilon^{(i)}}\rangle, \tag{10}$$

where C is a constant factor obtained by replacing r_{12} to an average value. Since the $2s$ and continuum orbitals are very diffuse, anisotropy of the ionization width is strongly governed by the compact He $1s$ and ionized molecular orbitals. Thus, the following equation for the estimation of ionization width into ith ionic state was used in the present study:

$$\Gamma^{(i)}=k^{(i)}|\langle\phi_i|\chi_{1s}\rangle|^2, \tag{11}$$

where $k^{(i)}$ is a parameter to be determined to reproduce observed branching ratios. SCF calculations with 6-311++G** basis set were performed to obtain the orbital functions for the isolated benzene molecule and a He atom.

C. Classical trajectory calculations and optimizations

CEDPICS was obtained by the following way.[31,32,34–37] Initial rotational energies of the molecule were generated so as to fit with the Boltzmann distribution at 300 K, and the impact parameter b was set randomly from 0 to 10 Å. The relative motion between the center of mass of the molecule and the He*($2\,^3S$) atom was determined by the equations of motion. At each trajectory step of an interval dt, transition probabilities $P^{(i)}(t)dt$ into each ionic state i were expressed by

$$P^{(i)}(t)dt=S(t)\frac{\Gamma^{(i)}}{\hbar}dt, \tag{12}$$

$$S(t)=1-\sum_i P_{\rm int}^{(i)}(t), \tag{13}$$

where the survival fraction $S(t)$ is the probability of He*($2\,^3S$) surviving in the excited state at a certain time t and then $P_{\rm int}^{(i)}$ represents the integrated partial ionization probability before time t. After 5000 trajectories were calculated with various initial parameters for initial collision energy, the partial ionization cross section $\sigma^{(i)}$ was obtained from the partial ionization probability $P^{(i)}$ of a trajectory,

$$\sigma^{(i)}=\int_0^\infty 2\pi b P^{(i)}db. \tag{14}$$

C_i in Eq. (6) and $k^{(i)}$ in Eq. (11) were optimized by a nonlinear least-squares method, so as to obtain good agreement between observed and calculated CEDPICS.

IV. RESULTS

Figure 3 shows potential energy curves of some selected directions. The definitions of θ and ϕ are also displayed and R indicates the distance between a He*($2\,^3S$) atom and the center of mass of a benzene molecule. The obtained potentials V^* are drawn with solid lines and the Li model potentials $V_{\rm Li}$ are shown with broken lines. Figure 4 shows obtained $V^*(R,\theta,\phi)$ contour maps of a He*($2\,^3S$) atom on (a) σ_h ($\theta=90°$) and (b) σ_v ($\phi=30°$) planes of a C_6H_6 molecule. The spacing of the contour lines is 20 meV for negative values from -100 meV to -20 meV and 100 meV for positive values from 0 meV to 800 meV, respectively. The optimized parameters for potential correction terms in Eq. (6) as well as $k^{(i)}$ in Eq. (11) are listed in Table I. The most stable geometry for He*($2\,^3S$)+C_6H_6 are also listed in Table I. Uncertainties of the potential parameters were estimated from errors of experimental slope values ($\Delta m=\pm 0.03$) of $\log\sigma^{(i)}$ versus $\log E_c$ plots, and they are shown in parentheses.

Figure 5 shows $\log\sigma^{(i)}$ versus $\log E_c$ plots of CEDPICS for He*($2\,^3S$)+C_6H_6. Observed partial cross sections for He*($2\,^3S$)+C_6H_6 were plotted with circles. Calculated CEDPICS curves are shown with solid lines for the use of V^* and dashed lines for $V_{\rm Li}$. Electron density contour maps for respective MOs are also shown in Fig. 5, in which the thick solid line in the maps represents the molecular surface estimated from van der Waals radii of component atoms. The cutting planes of the electron densities for C_6H_6 are 1.0 Å away from the σ_h plane of a benzene molecule.

In PIES of He*($2\,^3S$)+C_6H_6 as shown in Fig. 1, the satellite bands (S_1, S_2', and S_2) were observed[11,17,45] which

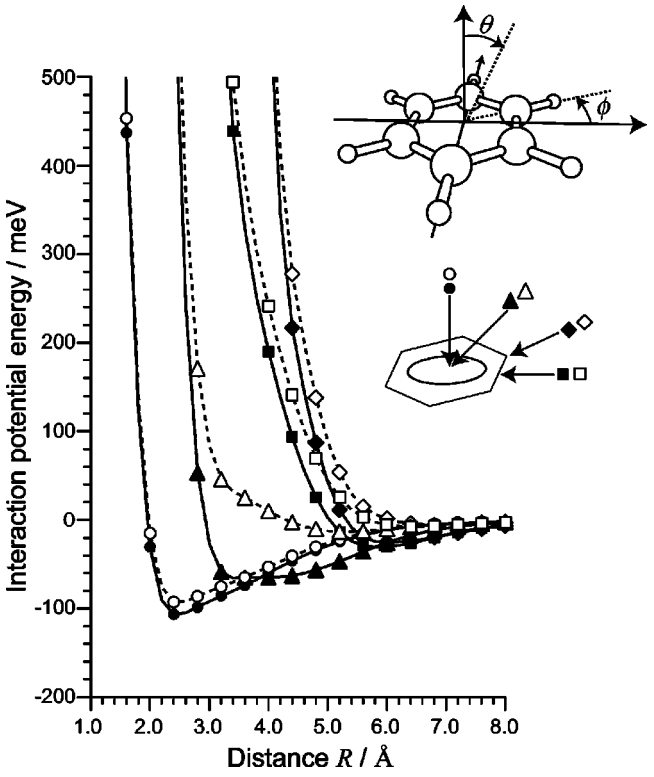

FIG. 3. Interaction potential energy curves of V^* for $He^*(2\,^3S)+C_6H_6$ (solid lines) and V_{Li} for $Li+C_6H_6$ (broken lines). Different directional approaches are represented with circles ($\theta=0°$), triangles ($\theta=45°$, $\phi=0°$), squares ($\theta=90°$, $\phi=0°$,), and diamonds ($\theta=90°$, $\phi=30°$). R represents the distance between a $He^*(2\,^3S)$ atom and the center of mass of a benzene molecule. Optimized parameter sets are listed in Table II.

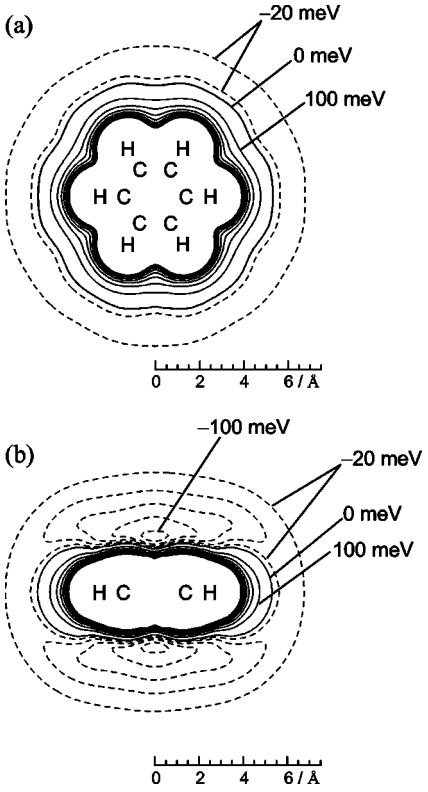

FIG. 4. Contour maps of V^* for $He^*(2\,^3S)+C_6H_6$; a $He^*(2\,^3S)$ atom is on the (a) σ_h ($\theta=90°$) and (b) σ_v ($\phi=30°$) planes of a C_6H_6 molecule. The spacing of the contour lines is 20 meV for negative values from -100 meV to -20 meV and 100 meV for positive values from 0 meV to 800 meV, respectively.

stem from the many-body effect of the ionization process different from the electron exchange type one (see Sec. II B). Moreover, the C_{2s} ($^2E_{2g}$) band is known to be enhanced by the excitation energy transfer from He* to a target molecule followed by the autoionization.[11,46] In our treatment of ionization width, these satellite bands and C_{2s} band were not considered, and trajectory calculations were performed without taking account of their contributions. However, some findings on the assignments were remarked from energy dependence of satellite bands intensities that will be discussed in Sec. V A. Although absolute values of ionization cross sections cannot be obtained by our apparatus, a pulse radiolysis experiment[47] predicted the total deexcitation cross section for $He^*(2\,^3S)+C_6H_6$ is ca. 85 $Å^2$ at $E_c=33$ meV which must contain the contributions from satellite and C_{2s} bands. Calculated total ionization cross section except for satellites and C_{2s} bands is estimated to be ca. 60 $Å^2$ at $E_c=33$ meV, which is consistent with the reported value[47] in taking account for the absence of the contributions from satellite and C_{2s} bands. However, 2D-PIES data at lower energy region will enable us to determine more reasonable values for partial ionization cross sections by comparison with the reported total cross section. Table II shows average slope values m of $\log \sigma^{(i)}$ versus $\log E_c$ plots in the E_c range (100–300 meV), which were obtained by a linear approximation of

TABLE I. Optimized parameters C_i in the correction term of $\Sigma_i C_i|\langle\phi_i|\chi_s\rangle|^2$ and $k^{(i)}$ parameters for ionization widths (see text) for $C_6H_6+He^*(2\,^3S)$. Uncertainties of C_i for obtained V^* estimated from errors of experimental slope values ($\Delta m=\pm0.03$) are shown in parentheses. Optimized parameters (D_e, R_e, and θ_e) for a complex of $He^*(2\,^3S)+C_6H_6$ are given in the bottom.

ζ (bohr^{-1})	0.575
C_3 (meV)	101 (±28)
C_2 (meV)	142 (±7)
C_1 (meV)	1844 (±15)
C_1 (meV)	1501 (±393)
C_2 (meV)	1789 (±602)
C_3 (meV)	71 (±307)
C_4 (meV)	257 (±301)
C_5 (meV)	1704 (±340)
$k^{(X)}$ (eV)	0.823 (±0.13)
$k^{(A)}$ (eV)	1.71 (±0.34)
$k^{(B)}$ (eV)	1.23 (±0.20)
$k^{(C)}$ (eV)	2.83 (±0.47)
$k^{(D)}$ (eV)	23.6 (±3.6)
$k^{(E)}$ (eV)	3.44 (±0.69)
$k^{(F)}$ (eV)	6.97 (±1.1)
D_e (meV)	107 (±18)
R_e (Å)	2.40 (±0.3)
θ_e (deg)	0

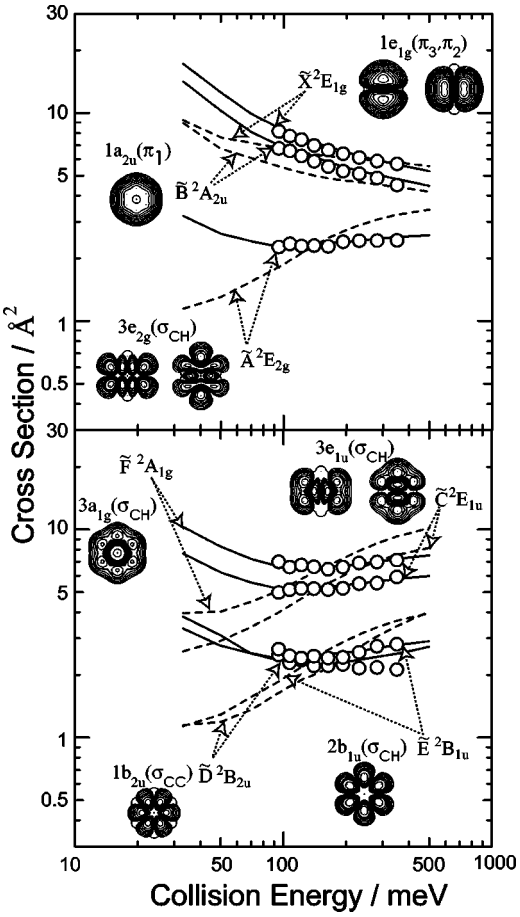

FIG. 5. Observed and calculated CEDPICS for $He^*(2\,^3S)+C_6H_6$; observed CEDPICS are plotted with circles and calculated CEDPICS curves obtained by the present trajectory calculations are shown with solid lines for V^* [Eqs. (6) and (7)] and dashed lines for V_{Li}.

CEDPICS in log-log plot. Obtained slope values of CEDPICS almost agree with previous ones[17] except for $\tilde{C}\,^2E_{1u}$, S_1, and $\tilde{F}\,^2A_{1g}$. The calculated results using the Li model potentials V_{Li} are shown with Calc. 1 and those using the overlap expansion potentials V^* are listed in Calc. 2.

V. DISCUSSION

A. CEDPICS and the potentials

In the present study, two satellite bands S_1 and S_2 which were previously observed in PIES (Ref. 45) were also observed in 2D-PIES around $E_e \sim 3.6$ eV and ~ 1.7 eV, respectively. By the deconvolutions of CERPIES, the additional satellite band S_2' was also found in 2D-PIES around $E_e \sim 2.1$ eV. S_1 band was assigned to the ionization from the $1e_{1g}(\pi_2,\pi_3)$ orbitals associated with the $\pi(1e_{1g}) - \pi^*(1e_{2u})$ excitation,[45] since the binding energy for the S_1 band (16.1 eV) is in good agreement with the summation of the ionization potential (IP) of the $1e_{1g}(\pi_2,\pi_3)$ electron (9.25 eV) (Ref. 39) plus the $\pi(1e_{1g})-\pi^*(1e_{2u})$ transition energy (6.95 eV).[48] Green's function method[49] assigned the S_1 band to $^2A_{2u}$ state which originates from the interaction of the $1a_{2u}(\pi_1)$ hole and the $(1e_{1g})^{-2}(1e_{2u})^1$ configurations, and the theoretically predicted IP for $^2A_{2u}$ state (16.69 eV) was in good agreement with the observed one. Moreover, collision-energy dependence of the S_1 band intensity showed negative slope,[11,17] which support the assignment based on the similarity in the slope of CEDPICS with the $1e_{1g}(\pi_2,\pi_3)$ orbitals. In the present study, similar slope of CEDPICS between S_1 and $1e_{1g}(\pi_2,\pi_3)$ orbitals was also obtained. Another satellite band S_2 has not ever been discussed with CEDPICS, although it was observed in PIES.[45] In this study, the slope of CEDPICS for S_2 band was reported. As shown in Table II, this slope is similar to that of σ bands rather than π bands, which imply S_2 band originates from a σ orbital ionization. Theoretical ionization spectra obtained by Green's function method[50] showed a shoulder in the higher electron energy of $\tilde{G}\,^2E_{2g}$ state. According to Green's function calculations,[49,50] this $^2E_{2g}$ state consists of several satellite states that originate from ionization of the $2e_{2g}$ orbital, and the three major leading configurations are $(2e_{2g})^{-1}$, $(3e_{1u})^{-1}(1e_{1g})^{-1}(1e_{2u})^1$, and $(1e_{1g})^{-2}(4a_{1g})^1$. There are three $^2E_{2g}$ states with pole strengths of the order of 0.10 and larger, and these states correspond to S_2', S_2, and $\tilde{G}\,^2E_{2g}$ states. The result of CEDPICS can support this assignment.

As can be seen in Fig. 5, calculated CEDPICS curves by

TABLE II. The slopes m of the $\log\sigma - \log E_c$ plots in CEDPICS of $He^*(2\,^3S)+C_6H_6$ in the collision-energy range from 90 to 300 meV.

Molecule	Ionic state	MO	Expt.	Calc. 1 (V_{Li})	Calc. 2 (V^*)
C_6H_6	$\tilde{X}\,^2E_{1g}$	$1e_{1g}(\pi_2,\pi_3)$	-0.29 ± 0.03	-0.13	-0.32
	$\tilde{A}\,^2E_{2g}$	$3e_{2g}(\sigma_{CH})$	0.07 ± 0.06	0.49	0.08
	$\tilde{B}\,^2A_{2u}$	$1a_{2u}(\pi_1)$	-0.32 ± 0.01	-0.18	-0.31
	$\tilde{C}\,^2E_{1u}$	$3e_{1u}(\sigma_{CH})$	0.09 ± 0.06	0.53	0.09
	$\tilde{D}\,^2B_{2u}$	$1b_{2u}(\sigma_{CC})$	-0.02 ± 0.01	0.57	0.07
	$\tilde{E}\,^2B_{1u}$	$2b_{1u}(\sigma_{CH})$	0.00 ± 0.06	0.56	0.11
	$S_1\,^2A_{2u}$	$(1e_{1g})^{-2}(1e_{2u})^1$	-0.21 ± 0.02	⋯	⋯
	$\tilde{F}\,^2A_{1g}$	$3a_{1g}(\sigma_{CH})$	0.03 ± 0.03	0.49	0.06
	S_2'		-0.11 ± 0.05	⋯	⋯
	$S_2\,^2E_{2g}$		0.03 ± 0.05	⋯	⋯
	$\tilde{G}\,^2E_{2g}$	$2e_{2g}(C_{2s})$	0.05 ± 0.03	⋯	⋯

the optimized potentials V^* as well as branching ratios are in excellent agreement with the experiments, whereas those by V_{Li} are far from satisfactory. Table II shows a considerable improvement of calculated CEDPICS by the potential optimizations. Measured partial cross sections show smooth energy dependence, and no quantum behavior could be observed. Therefore, reasonable interaction potential energy surface can be addressed within the use of classical trajectories. For $\tilde{D}\,^2B_{2u}$ state, the calculated CEDPICS slightly deviates from the experiment due to large experimental errors in estimating partial cross sections of a embedded band (See Fig. 1). In Fig. 5, CEDPICS curves for $\tilde{X}$ and $\tilde{B}$ states corresponding to ionization from π orbitals ($1e_{1g}$,$1a_{2u}$) decrease with the increase of E_c in connection with the attractive potentials around the regions where the π electrons are largely distributed. The similarity between two curves for the π states is due to the similar spatial electron distributions and PIES could be reasonably deconvoluted. Observed CEDPICS curves for the σ ($\tilde{A}$, $\tilde{C}$, $\tilde{D}$, $\tilde{E}$, and $\tilde{F}$) bands are nearly flat or slightly positive. Calculated curves for σ orbitals by V^* indicate that repulsive interactions are involved at high E_c regions, whereas attractive interactions become dominant at low E_c regions. Extending features of attractive well regions can be seen in Fig. 4. The difference of CEDPICS between σ and π orbitals which reflects the anisotropy of the potential surface was consistent with the obtained potential energy surface and well reproduced with the present classical trajectory calculations. Contour surfaces of -20 meV (ca. -0.5 kcal/mol) completely wrap the benzene molecule, surfaces of -50 meV (ca. -1.2 kcal/mol) nearly sandwich the benzene molecule including hydrogen regions, and surfaces of -80 meV (ca. -1.8 kcal/mol) just cover the carbon hexagon.

The deepest point of the attractive potential well [the structure of a $He^*(2\,^3S)+C_6H_6$ complex] is located at a distance of $R_e=2.40$ Å on the sixfold axis ($\theta=0°$) from the center of a benzene molecule, and the well depth (the binding energy) is 107 meV (2.47 kcal/mol), which is of the order of hydrogen bonding. This direction of the attractive well is the same as those for $Li+C_6H_6$ (Ref. 3) and is much larger than that for $He+C_6H_6$.[6,51] It was found that an excitation of a He atom leads to considerable increase of stabilization energy with a benzene molecule around the π electron area. For the parallel directions to the benzene ring [Fig. 4(a)], the interaction potentials are almost repulsive except for weak van der Waals interaction of ca. -20 meV. As can be seen from Fig. 4, sizes of repulsive surfaces diminish on going from 0 meV to 800 meV, where the repulsive surface nearly converges to the hard-core limit. The diameter of a benzene ring as probed by a $He^*(2\,^3S)$ atom is ca. 7.5-10 Å, and the thickness is ca. 3.1-4.4 Å.

Interesting features of the potential optimization from V_{Li} to V^* may be summarized as follows:

(1) Potential wells around the π electron area vertical to the molecular plane are considerably widened, though the depths are only slightly deepened.

(2) Long-range attractive interactions are augmented typically by ca. -1 kcal/mol at $R=6$ Å.

(3) Repulsive walls are slightly hardened.

From derivatives of obtained potentials with respect to geometrical parameters, forces exerting on the He* atom around a benzene molecule can be obtained. Attractive forces along the symmetry axis are ca. 50–55 pN in a wide range between $R=2.7-4.5$ Å. Attractive forces in the molecular plane are ca. 30–35 pN at $R=5.7-6.6$ Å. This means attractive forces are much stronger in the vertical directions.

B. Obtained potential parameters and characteristic features

The physical significance of the potential correction can be considered with the optimized parameters in Table I. The ζ value of 0.575 bohr^{-1} was found to be satisfactory, which implies that the correction terms in Eq. (6) represent orbital interactions between target MOs and a He* $2s$ orbital and not for the inner $1s$ orbital in a He* atom. Since $He^*(2\,^3S)$ has a smaller ionization potential (4.768 eV) than Li (5.392 eV), the $2s$ electron-energy level of $He^*(2\,^3S)$ is higher than that of $Li(2\,^2S)$. According to the concept of orbital interactions, He* $2s$ orbital can be stabilized by unoccupied molecular orbitals of a target molecule and the magnitude of the stabilization is proportional to the inverse of the orbital energy difference. Contributions of energy lowering in the Li model potential V_{Li} are thus expected to be underestimated for unoccupied MOs. As can be seen in Table I, the lowest unoccupied molecular orbital (LUMO) (C_1) shows a large positive contribution to the correction, which considerably lowers the Li model potential at around $\theta=45°$ in Fig. 4, and the magnitude shows a decreasing order from LUMO (C_1) to the higher levels (C_2, C_3). It should be noted that LUMOs $1e_{2u}(\pi_4,\pi_5)$ have electron distributions not on the sixfold symmetry axis but nearly on the skeletal carbon atoms, as can be seen in Fig. 2. Small but significant positive contributions C_2 and C_3 from unoccupied $4a_{1g}$ and $4e_{1u}$ orbitals should also be noted, because these σ orbitals are so diffuse that they may contribute substantial corrections of long-range interactions. Although long-range interaction terms directly related to the polarizability were not included in the present potential corrections, the overlap with unoccupied MOs such as $4a_{1g}$ and $4e_{1u}$ may correct indirectly long-range interactions because of the use of diffuse basis sets.

Large positive contributions C_1, C_2, and C_5 from occupied orbitals of $1e_{1g}(\pi_2,\pi_3)$, $3e_{2g}(\sigma_{CH})$, and $1b_{2u}(\sigma_{CC})$ should also be noted. It is interesting that these orbitals correspond to different area around the molecule, regions at vertical directions to the ring, around hydrogen atoms, and around CC bonds, respectively. This feature may be partly related to that attractive interactions are in all area underestimated in V_{Li}, because of insufficient electron correlation effects in the present calculations (MP2/6-311++G**). Electron correlation effects play an essential role in attractive interaction that is caused by induced dipole and induced dipole interactions. In this case, $2s$-$2p$ hybridization effects in the Li/He* atom should be considered. Since the $2s$-$2p$ energy gap for $He^*(2\,^3S)$ (1.114 eV) is smaller than that for $Li(2\,^2S)$ (1.848 eV), $He^*(2\,^3S)$ is more easily polarized by the $2s$-$2p$ hybridization effect.

Highest occupied molecular orbital (HOMO) coefficient of acetylene has negative contribution to the energy correction whereas those of N_2 and CO has positive.[36] This was interpreted by the overestimation of the stabilization for HOMO energy level, because Li $2s$ orbital can more easily interact with target occupied MOs than He* $2s$. Since acetylene has small ionization potential (IP=11.40 eV),[39] the magnitude of this correction became larger than $2s$-$2p$ hybridization corrections. However, HOMO coefficient of a benzene molecule positively contributes to energy lowering, although benzene has smaller IP (9.25 eV) (Ref. 39) than acetylene. The MO levels of benzene are weakly affected by the presence of He* $2s$ orbital, because the overestimation of energy stabilization is suppressed by intramolecular orbital mixings. The energy difference of HOMO-next-HOMO calculated with 6-311++G** basis is 4.27 eV for benzene which is much smaller than for acetylene (7.38 eV). On the other hand, the magnitude of the $2s$-$2p$ hybridization will become important for energy correction. It is of note that benzene can more strongly attract a He*($2\,^3S$) atom than acetylene, which is well reflected in the slope of CEDPICS for π orbitals.

The $k^{(i)}$ parameters determine the absolute values of partial cross sections and hardly affect their collision-energy dependences. The relative magnitude of obtained $k^{(i)}$ is roughly related to the ionization potential. The larger the ionization potential of the ionized electron (the smaller the kinetic energy of ejected electron E_e) the corresponding values for $k^{(i)}$ becomes larger. This tendency may be related to a factor of $E_e^{-1/2}$ in a formula for the ionization width.[52] Discrepancy in $\tilde{D}\,^2B_{2u}$ state is due to the difficulty in obtaining band intensity. Since $^2A_{2u}$ state contributes the S_1 band, the $k^{(i)}$ parameter for $\tilde{B}\,^2A_{2u}$ state must be underestimated.

VI. CONCLUSION

Anisotropic interaction potential energy surface of benzene (C_6H_6) with a metastable He*($2\,^3S$) atom was investigated by collision-energy/electron-energy-resolved two-dimensional Penning ionization electron spectroscopy combined with optimization of the *ab initio* model potentials. In order to estimate CEDPICS as well as ionization branching ratios, asymmetric Gaussian deconvolutions were applied to observed collision-energy-resolved Penning ionization electron spectra. Observed slopes in log-log plot of CEDPICS were compared with those estimated from electron-energy integrations around peak positions which were obtained in the ordinary way, and the slopes were well reproduced within experimental errors. Observed partial ionization cross sections showed apparently different energy dependence on whether ionized molecular orbital has π or σ characters. Although *ab initio* Li model potentials based on the similarity between a He*($2\,^3S$) atom and a Li($2\,^2S$) atom were used for classical trajectory calculations, the interaction potential surface was found to be disappointing to reproduce observed CEDPICS. The optimization was performed to modify the model potentials by correction terms composed of overlap integrals between the orbitals of the interacting system. The results of trajectory calculations were dramatically improved by the potential optimizations. Important contributions to corrections were found to be due to orbital interactions between unoccupied molecular orbitals and the He* $2s$ orbital. The overlap expansion method was successful in modifying *ab initio* model potentials effectively and efficiently, and it enables us to understand the physical meaning of potential corrections.

A benzene molecule was found to attract a He*($2\,^3S$) atom widely at the region where π electrons distribute. A complex of a C_6H_6 molecule with a He*($2\,^3S$) atom has a binding of 107 meV (2.47 kcal/mol) at a distance of 2.40 Å on the sixfold symmetry axis which is much larger than the case of acetylene (56.5 meV).[36] Attractive forces acting on He* atom around a benzene molecule are strong as ca. 50–55 pN in a wide range between R=2.7–4.5 Å in the vertical directions. This means that mechanical characteristics of the molecular surface of benzene are highly anisotropic.

ACKNOWLEDGMENTS

The present work was supported by a Grant-in-Aid for Scientific Research from the Japanese Ministry of Education, Science, and Culture. The authors acknowledge the Computer Center of the Institute for Molecular Science, for the use of the Fujitsu VPP5000 computer. M.Y. is supported by the Research Fellowship of the Japan Society for the Promotion of Science for Young Scientists. The authors are grateful to Dr. Y. Yamakita and T. Horio for their helpful discussion on experimental data.

[1] L. Manceron and L. Andrews, J. Am. Chem. Soc. **110**, 3840 (1988).
[2] S. Irle and H. Lischka, J. Mol. Struct. **364**, 15 (1996).
[3] J. M. Vollmer, A. K. Kandalam, and L. A. Curtiss, J. Phys. Chem. A **106**, 9533 (2002).
[4] D. Cappelletti, M. Bartolomei, F. Pirani, and V. Aquilanti, J. Phys. Chem. A **106**, 10764 (2002).
[5] F. Pirani, D. Cappelletti, and G. Liuti, Chem. Phys. Lett. **350**, 286 (2001).
[6] F. Pirani, M. Porrini, S. Cavalli, M. Bartolomei, and D. Cappelleti, Chem. Phys. Lett. **367**, 405 (2003).
[7] K. Ohno, H. Yamakado, T. Ogawa, and T. Yamata, J. Chem. Phys. **105**, 7536 (1996).
[8] K. Mitsuke, T. Takami, and K. Ohno, J. Chem. Phys. **91**, 1618 (1989).
[9] K. Ohno, T. Takami, K. Mitsuke, and T. Ishida, J. Chem. Phys. **94**, 2675 (1991).
[10] D. C. Dunlavy, D. W. Martin, and P. E. Siska, J. Chem. Phys. **93**, 5347 (1990).
[11] T. Takami and K. Ohno, J. Chem. Phys. **96**, 6523 (1992).
[12] D. C. Dunlavy and P. E. Siska, J. Chem. Phys. **100**, 21 (1996).
[13] H. Hotop and A. Niehaus, Z. Phys. **228**, 68 (1969).
[14] K. Ohno, H. Mutoh, and Y. Harada, J. Am. Chem. Soc. **105**, 4555 (1983).
[15] K. Ohno, S. Matsumoto, and Y. Harada, J. Chem. Phys. **81**, 4447 (1984).
[16] A. Niehaus, Adv. Chem. Phys. **45**, 399 (1981).
[17] Y. Yamakita, M. Yamauchi, and K. Ohno, Chem. Phys. Lett. **322**, 189 (2000).
[18] T. Horio, R. Maruyama, N. Kishimoto, and K. Ohno, Chem. Phys. Lett. **384**, 73 (2004).
[19] N. Kishimoto, M. Furuhashi, and K. Ohno, J. Electron Spectrosc. Relat. Phenom. **113**, 35 (2000).
[20] K. Imura, N. Kishimoto, and K. Ohno, J. Phys. Chem. A **105**, 4189 (2001).
[21] K. Imura, N. Kishimoto, and K. Ohno, J. Phys. Chem. A **105**, 6073 (2001).
[22] K. Imura, N. Kishimoto, and K. Ohno, J. Phys. Chem. A **105**, 9111 (2001).
[23] K. Imura, N. Kishimoto, and K. Ohno, J. Phys. Chem. A **105**, 10781 (2001).
[24] W. H. Miller, J. Chem. Phys. **52**, 3563 (1970).
[25] J. S. Cohen and N. F. Lane, J. Chem. Phys. **66**, 586 (1977).
[26] T. Ishida and K. Horime, J. Chem. Phys. **105**, 5380 (1996).

[27] T. Ishida, J. Chem. Phys. **105**, 1392 (1996).
[28] M. Albertí, J. M. Lucas, B. Brunetti, F. Pirani, M. Stramaccia, M. Rosi, and F. Vecchiocattivi, J. Phys. Chem. A **104**, 1405 (2000).
[29] E. W. Rothe, R. H. Neynaber, and S. Trujillo, J. Chem. Phys. **42**, 3310 (1965).
[30] H. Hotop, T. E. Roth, M.-W. Ruf, and A. J. Yencha, Theor. Chem. Acc. **100**, 36 (1998).
[31] T. Ogawa and K. Ohno, J. Chem. Phys. **110**, 3773 (1999).
[32] T. Ogawa and K. Ohno, J. Phys. Chem. A **103**, 9925 (1999).
[33] M. Yamato, H. Ohoyama, and T. Kasai, J. Phys. Chem. A **105**, 2967 (2001).
[34] M. Yamazaki, S. Maeda, N. Kishimoto, and K. Ohno, Chem. Phys. Lett. **355**, 311 (2002).
[35] M. Yamazaki, S. Maeda, N. Kishimoto, and K. Ohno, J. Chem. Phys. **117**, 5707 (2002).
[36] S. Maeda, M. Yamazaki, N. Kishimoto, and K. Ohno, J. Chem. Phys. **120**, 781 (2004).
[37] N. Kishimoto, T. Horio, S. Maeda, and K. Ohno, Chem. Phys. Lett. **379**, 332 (2003).
[38] J. L. Gardner and J. A. R Samson, J. Electron Spectrosc. Relat. Phenom. **8**, 469 (1976).
[39] K. Kimura, S. Katsumata, Y. Achiba, T. Yamazaki, and S. Iwata, *Handbook of He I Photoelectron Spectra of Fundamental Organic Molecules*, (Japan Scientific, Tokyo, 1981).
[40] M. J. Frisch, G. W. Trucks, H. B. Schlegel, *et al.*, GAUSSIAN94, Revision D.4, Gaussian, Inc., Pittsburgh PA, 1995.
[41] S. F. Boys and F. Bernardi, Mol. Phys. **19**, 553 (1970).
[42] W. H. Miller and H. Morgner, J. Chem. Phys. **67**, 4923 (1977).
[43] R. S. Mulliken, J. Chim. Phys. Phys.-Chim. Biol. **46**, 497 (1949).
[44] Vu. N. Demikov, Sov. Phys. JETP **18**, 138 (1964).
[45] S. Masuda, M. Aoyama, K. Ohno, and Y. Harada, Phys. Rev. Lett. **65**, 3257 (1990).
[46] T. Takami, K. Mitsuke, and K. Ohno, J. Chem. Phys. **95**, 918 (1991).
[47] T. Ueno and Y. Hatano, Oyo Butsuri **47**, 1006 (1978).
[48] J. P. Doering, J. Chem. Phys. **51**, 2866 (1969).
[49] H.-G. Weikert and L. S. Cederbaum, Chem. Phys. Lett. **237**, 1 (1995).
[50] M. S. Deleuze, A. B. Trofimov, and L. S. Cederbaum, J. Chem. Phys. **115**, 5859 (2001).
[51] P. Hobza, O. Bludský, H. L. Selzle, and E. W. Schlag, J. Chem. Phys. **97**, 335 (1992).
[52] W. H. Miller, C. A. Slocomb, and H. F. Schaefer III, J. Chem. Phys. **56**, 1347 (1972).